Spin-Canting and Magnetic Anisotropy in Ultrasmall CoFe 2 O 4 Nanoparticles

9 **AUTHORS**, INCLUDING:

Davide Peddis
Italian National Research Council
64 PUBLICATIONS **820** CITATIONS

SEE PROFILE

Carla Cannas
Università degli studi di Cagliari
100 PUBLICATIONS **1,716** CITATIONS

SEE PROFILE

Anna Musinu
Università degli studi di Cagliari
121 PUBLICATIONS **2,687** CITATIONS

SEE PROFILE

Giorgio Piccaluga
Università degli studi di Cagliari
141 PUBLICATIONS **3,374** CITATIONS

SEE PROFILE

Spin-Canting and Magnetic Anisotropy in Ultrasmall CoFe$_2$O$_4$ Nanoparticles

D. Peddis,*,†,‡ M. V. Mansilla,† S. Mørup,§ C. Cannas,‡ A. Musinu,‡ G. Piccaluga,‡ F. D'Orazio,∥ F. Lucari,⊥ and D. Fiorani†

Istituto di Struttura della Materia-CNR, C.P. 10, 00016 Monterotondo Stazione, Roma, Italy, Dipartimento di Scienze Chimiche, Citt. Università di Monserrato, Bivio per Sestu, 09042 Monserrato (Ca), Italy, Department of Physics, Technical University of Denmark, DK-2800 Kgs. Lyngby, Denmark, and CNISM and CNR-INFM at Dip di Fisica Università di L'Aquila, 67100, Coppito L'Aquila, Italy

The magnetic properties of cobalt ferrite nanoparticles dispersed in a silica matrix in samples with different concentrations (5 and 10 wt % CoFe$_2$O$_4$) and same particle size (3 nm) were studied by magnetization, DC and AC susceptibility, and Mössbauer spectroscopy measurements. The results indicate that the particles are very weakly interacting. The magnetic properties (saturation magnetization, anisotropy constant, and spin-canting) are discussed in relation to the cation distribution.

1. Introduction

Nanoparticles are unique complex physical objects whose physical properties differ greatly from their parent massive materials.[1] The magnetic properties are particularly sensitive to the particle size, being determined by finite size effects on the core properties, related to the reduced number of spins cooperatively linked within the particle, and by surface effects, becoming more important as the particle size decreases.[2,3] The modification of the structural and electronic properties near and at the particle surface results in breaking of lattice symmetry and broken bonds, which give rise to site-specific surface anisotropy, weakened exchange coupling, magnetic frustration, and spin disorder.[4] Such disorder may propagate from the surface to the particle core, such that the picture of the particle as a perfectly ordered single domain, whose spins rotate in a synchronous way as a large single spin, is no longer valid.[5–8] Interparticle interactions also play an important role in determining the magnetic properties of an assembly of particles.[9–12]

In spinel oxide ferrite (Me^{II}Fe$_2$O$_4$) nanoparticles, other effects are also present. The cation distribution between the tetrahedral (A) and octahedral (B) sites affects the spin alignment and the degree of spin-canting. The cation distribution can be size-dependent and may also depend on the synthesis method.

In a previous study,[7] we investigated the particle size (from 7 to 28 nm) and concentration dependence (from 15 to 50 wt %) of the magnetic properties of CoFe$_2$O$_4$ nanoparticles dispersed in a silica matrix. The results indicated a superparamagnetic behavior of nanoparticles, with weak interactions slightly increasing with particle size and concentration.

To investigate the intercorrelation among the different factors affecting magnetic properties, we studied the magnetic behavior of two CoFe$_2$O$_4$–silica nanocomposites with low particle concentration (5 and 10 wt %),[13] making interparticle interactions very weak. This allowed us to analyze single particle magnetic behavior. Moreover, since the particle size (∼3 nm)

and size distribution are the same, within the experimental error, in the two samples it was possible to perform a better investigation of the influence of cation distribution on spin-canting and magnetic anisotropy. Some previous results[7] obtained on a more concentrated sample (15 wt %) with bigger particles will be recalled to gain a better understanding on the interrelation between particle size, cation distribution, and spin-canting in CoFe$_2$O$_4$ nanoparticles.

2. Experimental Section

The synthesis and a detailed morphological and structural characterization of the samples are given elsewhere.[13] The samples consist of powders, coming from an autocombustion reaction followed by heat treatments. The temperature was raised to 900 °C with steps of 100 °C, and the samples were kept for 1 h at each temperature. The samples with 5, 10, and 15% by weight are identified as N5, N10, and N15, respectively. The particle size distributions for the N5 and N10 samples (Figure 1a,b, bars), obtained from HRTEM, are fitted with log-normal functions (Figure 1a,b, lines), and the mean particle sizes ($\langle D_{TEM} \rangle$) are reported in Table 1. The results of inductively coupled plasma analysis confirmed both the molar nominal ratio CoFe$_2$O$_4$/silica and the nominal composition of CoFe$_2$O$_4$.

DC magnetization measurements were performed using a Quantum Design SQUID magnetometer ($\mu_0 H_{max} = 5$ T). The samples in forms of powders were immobilized in an epoxy resin to prevent any movement of the nanoparticles during the measurements. AC susceptibility measurements were performed at different frequencies (5 Hz–10 kHz) as a function of temperature using a Lakeshore ACS 7000. All the magnetic measurements are normalized by mass of CoFe$_2$O$_4$.

Mössbauer spectra were obtained using constant acceleration spectrometers with 50 mCi sources of ^{57}Co in rhodium. The spectrometers were calibrated with a 12.5-μm α-Fe foil at room temperature, and isomer shifts are given with respect to that of α-Fe at room temperature. The spectra measured below 80 K were obtained using a closed cycle helium refrigerator from APD Cryogenics, Inc. and the spectra between 80 and 295 K using a liquid nitrogen cryostat. Spectra in a magnetic field of 6 T, applied parallel to the γ-ray direction, were obtained using a liquid helium cryostat with a superconducting coil.

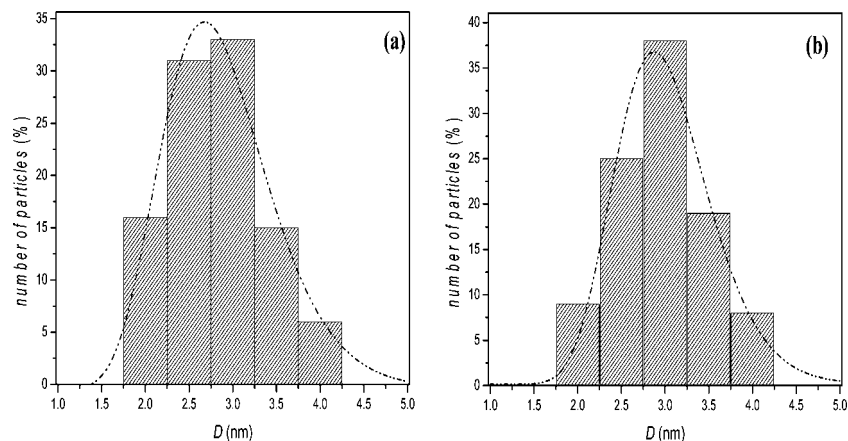* Corresponding author. Telephone: +39 06-90672315. Fax: +39 06-90672470.
† Istituto di Struttura della Materia-CNR.
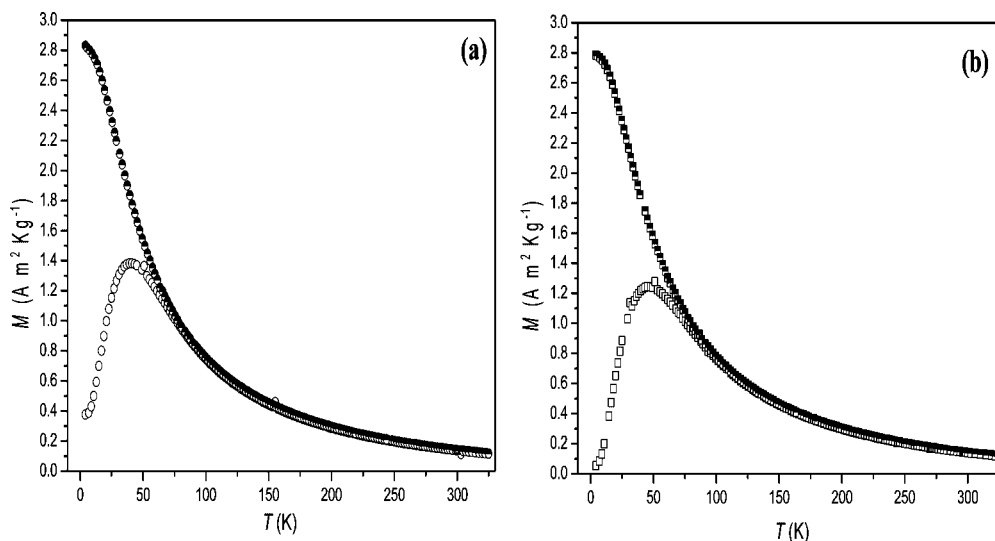‡ Citt. Università di Monserrato.
§ Technical University of Denmark.
∥ CNISM at Dip di Fisica Università di L'Aquila.
⊥ CNR-INFM at Dip di Fisica Università di L'Aquila.

Figure 1. Particle size distribution for samples N5 (a) and N10 (b) derived from HRTEM analysis (bars) and fitted with log-normal functions (lines).

Figure 2. ZFC (empty symbols) and FC (full symbols) DC magnetizations for N5 (a, circles) and N10 (b, squares).

3. Results and Discussion

The results of zero-field-cooled (ZFC) and field-cooled (FC) magnetization measurements on N5 and N10 are shown in Figure 2a,b, respectively. The measurements were carried out as follows: first, the sample was cooled from 325 to 4.2 K in zero magnetic field, then a static magnetic field of 5 mT was applied, and M_{ZFC} was measured during warming from 4.2 to 325 K; finally, the sample was cooled to 4.2 K in the magnetic field, and M_{FC} was measured during the cooling. The behavior is typical of an assembly of superparamagnetic particles, whose moments block progressively with decreasing temperature, according to the distribution of their blocking temperatures. The continuous increase of M_{FC} with decreasing temperature gives a first qualitative hint about magnetic interparticle interactions, indicating that they are very weak in both samples. The ZFC magnetization curves present a maximum at a temperature (T_{max}), which is related to the average blocking temperature (T_B):

$$T_{max} = \beta\langle T_B\rangle \tag{1}$$

where β is a proportionality constant, depending on the type of size distribution. For a log-normal distribution, the value of β is typically in the range 1.5–2.5.[14] The blocking temperature is defined as the temperature for which the relaxation time is equal to the experimental time window (τ_m).

TABLE 1: Mean Particle Size from TEM Data ($\langle D_{TEM}\rangle$), Temperature Corresponding to the Maximum in ZFC Curve (T_{max}), Irreversibility Temperature (T_{irr}), Blocking Temperature from TRM Measurement (T_B^m), and Blocking Temperature from Mössbauer Spectroscopy (T_B^M)[a]

sample	abbreviation	$\langle D_{TEM}\rangle$ (nm)	T_{max} (K)	T_{irr} (K)	T_B^m (K)	T_B^M (K)
CoFe$_2$O$_4$/SiO$_2$ 5 wt %	N5	2.8(3)	41(1)	65(1)	17(1)	51(10)
CoFe$_2$O$_4$/SiO$_2$ 10 wt %	N10	2.9(3)	49(1)	73(1)	18(1)	80(10)
CoFe$_2$O$_4$/SiO$_2$ 15 wt %	N15	6.7(4)	53(2)	85(2)	26(1)	126(10)

[a] Uncertainties are given in parentheses in the last digit.

The superparamagnetic relaxation of an assembly of noninteracting nanoparticles can be described according to the Néel–Brown model[15] by the equation:

$$\tau = \tau_0 \exp\left(\frac{\Delta E_a}{k_B T}\right) \tag{2}$$

where τ is the superparamagnetic relaxation time (i.e., the average time between the reorientation of the magnetization direction), τ_0 is the characteristic relaxation time, T is the absolute temperature, and k_B is the Boltzmann constant. ΔE_a is
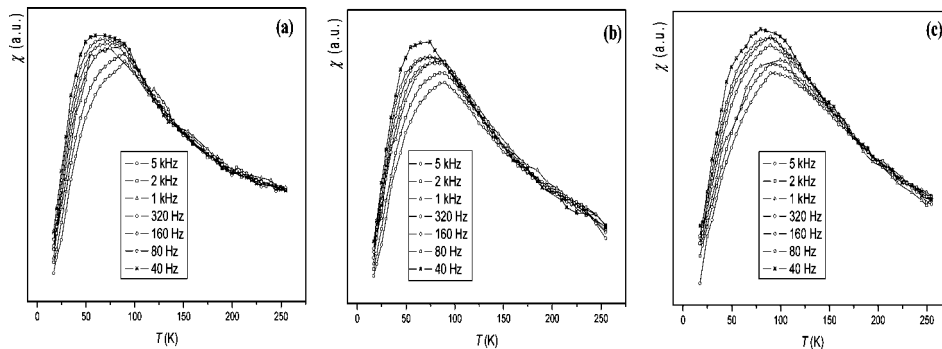
Figure 3. Temperature dependence of the in-phase component of the AC susceptibility (χ'_{AC}) at different frequencies for the samples N5 (a), N10 (b) and N15 (c).
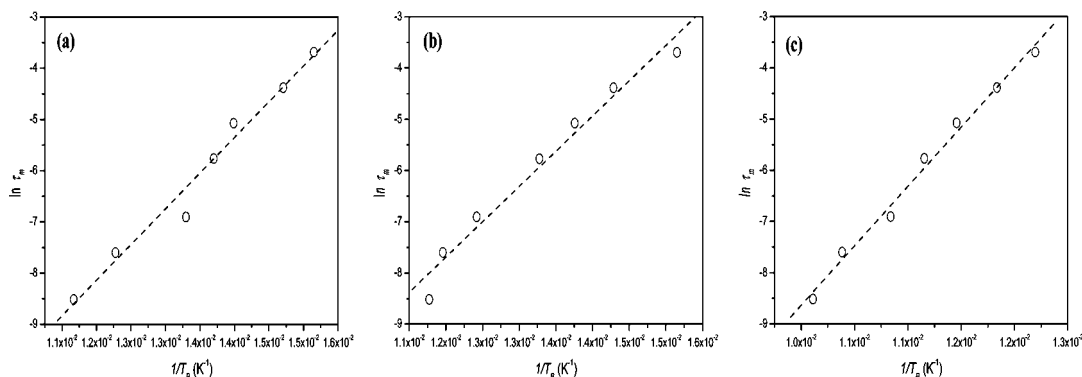
Figure 4. $\ln(\tau_m)$ vs ($1/T_B$) (○) with linear fit (solid line) for N5 (a), N10 (b), and N15 (c).

the magnetic anisotropy energy barrier that for uniaxial anisotropy is given by $\Delta E_a = KV$, where K is the magnetic anisotropy constant and V is the particle volume. The FC and ZFC curves split below a temperature called the irreversibility temperature (T_{irr}), which is associated with the blocking of the biggest particles.[16] We have taken T_{irr} as the temperature where the difference between M_{FC} and M_{ZFC}, normalized to its maximum value at the minimum temperature (4.2 K), becomes smaller than 3%.[17] The difference between T_{irr} and T_{max} provides a measure of the width of the blocking temperature distribution and then of the particle size distribution, assuming the same anisotropy constant and absence of interparticle interactions.[17] The values of T_{max} and T_{irr} are reported in Table 1; for comparison, the values for the sample N15 are also reported. Going from N5, N10 to N15, the values of T_{irr} and T_{max} cannot be explained by an anisotropy energy that is proportional to the volume, and other effects too seem to play an important role. For the sample N10, the values of T_{irr} and T_{max} are slightly higher than that for the N5 sample, but the difference $T_{irr} - T_{max}$ is equal in the two samples.

AC susceptibility measurements represent a very useful tool to study dynamical properties of magnetic nanoparticles. In Figure 3, the temperature dependence of the real part (χ'_{AC}) of the AC susceptibility measured at different frequencies for the samples N5 (Figure 3a), N10 (Figure 3b), and N15 (Figure 3c) are reported. At high temperatures, χ'_{AC} follows a Curie−Weiss law. With decreasing temperature, it deviates from this behavior and shows a maximum at a frequency-dependent temperature, increasing with increasing frequency. Since the variation of the measuring frequency (ν) corresponds to the change of the experimental time window ($\tau_m = 1/\nu$), it is possible to analyze the frequency dependence of the blocking temperature and then evaluate ΔE_a and τ_0 from the linear dependence between $\ln \tau_m$ and $1/T_B$ ($\ln \tau_m = \ln \tau_0 + \Delta E_a/k_B T_B$).

TABLE 2: Characteristic Relaxation Time (τ_0), Averaged Energy Barrier (ΔE_a), and Effective Anisotropy Constant ($\langle K_{eff} \rangle$) Obtained from AC Measurements[a]

sample	τ_0 (s)	ΔE (J)	$\langle K_{eff} \rangle$ (J/m^3)
N5	1.6×10^{-11}(1)	1.9×10^{-20}(1)	1.7×10^{6}(2)
N10	2.9×10^{-11}(1)	1.8×10^{-20}(1)	1.6×10^{6}(2)
N15	1.5×10^{-14}(1)	3.2×10^{-20}(1)	1.9×10^{5}(1)

[a] Uncertainties are given in parentheses in the last digit.

In all three samples, the frequency dependence of T_B is well described by the Arrhenius law (Figure 4). In Table 2, the values of ΔE_a and τ_0 are reported for all the samples. The estimated very low value of τ_0 for N15 can be ascribed to the influence of interparticle interactions, as reported in the literature.[18,19]

Taking $\langle V \rangle$ from TEM measurements, we can derive a mean value of the effective anisotropy constant, $\langle K_{eff} \rangle$ (including all the contributions) (Table 2). The $\langle K_{eff} \rangle$ values are much larger than the bulk value (3.0×10^5 J/m^3)[1,7] for N5 and N10, while it is of the same order of magnitude for N15. Thus, $\langle K_{eff} \rangle$ increases with decreasing particle size.

Thermoremanent magnetization (TRM) was measured by cooling the sample from 325 to 4.2 K in a magnetic field of 5 mT, then the field was turned off and the remanent magnetization was measured on warming up. Figure 5a shows TRM measurements for N10 and N5.

For an assembly of noninteracting particles, M_{TRM} is related to the distribution of anisotropy energy barriers:

$$M_{TRM} = M_{nr} \int_{\Delta E_c}^{\infty} f(\Delta E_a) \, dE \qquad (3)$$

where M_{nr} is the nonrelaxing component of the magnetization and ΔE_c is a critical value of energy, above which all the particles are blocked. The presence of a inferior limit (ΔE_c) in
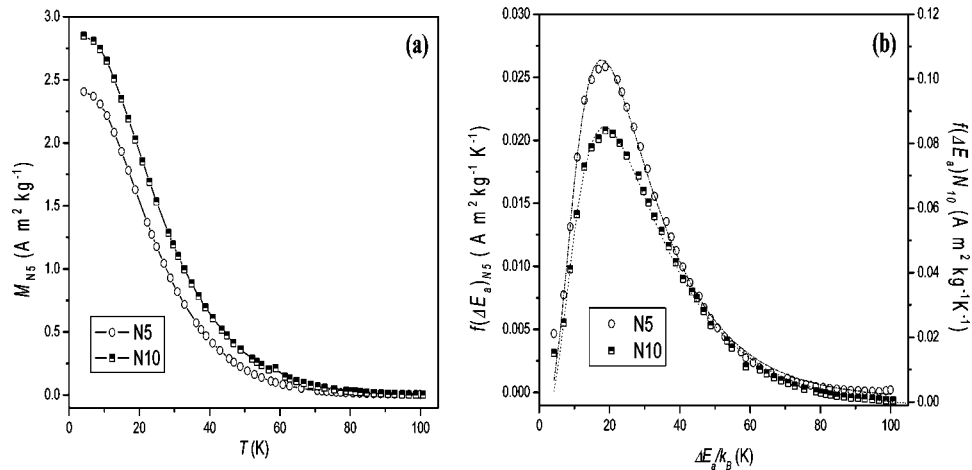
Figure 5. TRM measurements (a) and corresponding distribution of magnetic anisotropy energies (b) with cooling field of 5 mT for the samples N5 and N10. The left *y*-scale in (b) refers to N5 sample and the right one to N10 sample.
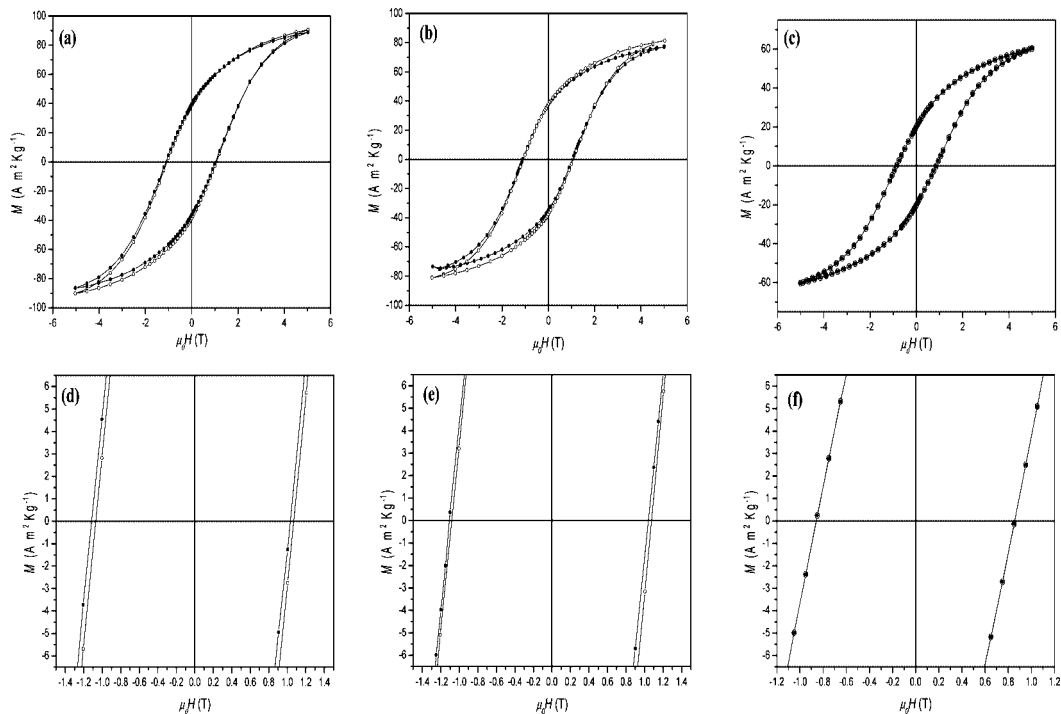
Figure 6. ZFC (○) and FC (●) hysteresis loops of the N5 (a), N10 (b), and N15 (c) samples. Details of ZFC and FC hysteresis loops for N5 (d), N10 (e), and N15 (f).

the integral means that, at a given temperature and for a given applied field, only the particles for which the energy barrier is higher than ΔE_c contribute to the measured M_{TRM}. The temperature derivative of M_{TRM} provides a determination of the energy barrier distribution and then of blocking temperatures.[20] Figure 5b shows the deduced distributions of blocking temperatures. The distributions are similar for the two samples and fit well with a log-normal function. In principle, the average blocking temperature (T_B^m) can be considered as the temperature at which 50% of the particles overcome their anisotropy energy barriers.[21,22] However, this would exclude a fraction of nanoparticles that are superparamagnetic even at 4.2 K. To avoid this problem, following a suggestion given in the literature,[22] the blocking temperature was defined as the temperature at which the magnetic anisotropy distribution has its maximum. The $\langle T_B \rangle$ values (Table 1) obtained from the measurements carried out with a cooling field of 5 mT are equal for the two

samples, $\langle T_B \rangle \approx (1/2)T_{max}$, in accordance with the typical β values (eq 1) reported in the literature for log-normal distributions of nanoparticle sizes.[14]

Hysteresis measurements (○ in Figure 6a−c) were carried out at 4.2 K (i.e., well below the blocking temperatures estimated from TRM and ZFC−FC measurements). The saturation magnetization (M_s), the remanent magnetization (M_r), the reduced remanent magnetization (M_r/M_s), and the coercive field ($\mu_0 H_c$) are reported in Table 3 for the three samples. The M_s value was obtained by fitting the high-field part of the hysteresis curve using the relation:[23]

$$M = M_s \times \left(1 - \frac{a}{H} - \frac{b}{H^2}\right) \qquad (4)$$

H is the field strength, and a and b are parameters determined by the fitting procedure. For the same particle size, M_r and $\mu_0 H_c$ are very similar, whereas M_s is larger for the most diluted

TABLE 3: Parameters Obtained from Hysteresis Loops at 4.2 K: Saturation Magnetization (M_s), Remanent Magnetization (M_r), Reduced Remanent Magnetization (M_r/M_s), Coercive Field ($\mu_0 H_c$), and Exchange Bias Field ($\mu_0 H_{EB}$)[a]

sample	M_s 4.2 K (A m² kg⁻¹)	M_r (A m² kg⁻¹)	M_r/M_s	$\mu_0 H_c$ (T)	$\mu_0 H_{EB}$ (mT)
N5	109(6)	38.6(1)	0.36(2)	1.07(5)	40.6(3)
N10	89(2)	36.6(1)	0.44(4)	1.18(4)	32.4(1)
N15	78(1)	20.0(1)	0.26(2)	0.87(1)	0

[a] Uncertainties are given in parentheses in the last digit.

sample, N5. Hysteresis loops were also measured on the N5, N10, and N15 samples after cooling in a field of 2 T (● in Figure 6a–c). For the N5 and N10 samples, a shift of the loop along the field axis is observed after field cooling, whereas the loop remains symmetric with respect to the origin for the sample N15. The shift, due to exchange bias, is usually quantified as the exchange bias field, defined as $H_{EB} = -(H_{right} + H_{left})/2$;[17] for N5 and N10 $\mu_0 H_{EB}$ at 4.2 K is, respectively, ~40 and ~30 mT (Table 3). The presence of exchange bias may be explained by interface exchange coupling between a ferrimagnetically ordered (although likely with some canting)[5,8] core and a magnetically disordered surface shell.[24] The lack of exchange bias in N15 may indicate that the surface shell contribution is negligible for bigger particles, although interparticle interactions also may play a role in decreasing the exchange bias effect.[17]

When an assembly of magnetic nanoparticles is studied by Mössbauer spectroscopy, the total spectrum is typically a superposition of magnetic (six lines) and quadrupole patterns (two lines). These two components are due to particles with superparamagnetic relaxation time that is long or short compared to the time scale of Mössbauer spectroscopy, respectively. The relative weight of the doublet increases with temperature. The blocking temperature in Mössbauer spectroscopy T_B^M can be defined as the temperature at which 50% of the spectral area is

magnetically split. This corresponds to an average relaxation time of around 5×10^{-9} s.[11]

The Mössbauer spectra for N5 and N10 in the temperature range 15–295 K are shown in Figure 7. The T_B^M values are reported in Table 1 together with the value for N15.[7] At low temperatures, the spectra are dominated by magnetic sextets with broad and asymmetric lines due to the presence of iron atoms in tetrahedral (A) and octahedral (B) sites. At 15 K, it was possible to make a good fit of the spectra with overlapping six line patterns corresponding to ⁵⁷Fe located in the B and A sites. Hyperfine field (B_{hf}) and isomer shift (δ) values for the iron atoms in the A and B sites for all the samples are compatible with the presence of cobalt ferrite.[25]

Mössbauer spectra of ferrites in large external magnetic field (B_{app}) permit us to obtain more information about the cationic distribution and the magnetic structure. When Mössbauer spectra of ferrites are obtained in a large magnetic field, the magnetic splitting of the A-site Fe³⁺ ions increases and the B-site splitting decreases. Therefore, the applied field makes it possible to separate the A and B patterns and to obtain information about the inversion degree.

For a thin absorber, the relative area of the six lines is given by 3:p:1:1:p:3, where

$$p = \frac{4 \sin^2 \theta}{1 + \cos^2 \theta} \tag{5}$$

and θ is the angle between the effective magnetic field (B_{efc}) at the nucleus and the γ-ray direction.[4,5,8] From eq 5 it is evident that, if B_{efc} is perfectly aligned with the γ-ray direction, the intensity of lines 2 and 5 vanishes. B_{hf}, B_{efc}, and B_{app} are related by the expression:[26]

$$B_{hf}^2 = B_{efc}^2 + B_{app}^2 - 2B_{efc}B_{app} \cos \theta \tag{6}$$

Figure 8 shows Mössbauer spectra of the samples N5 and N10 at 6 K, measured with a magnetic field of 6 T applied parallel to the γ-ray direction. The nonzero intensity of lines 2
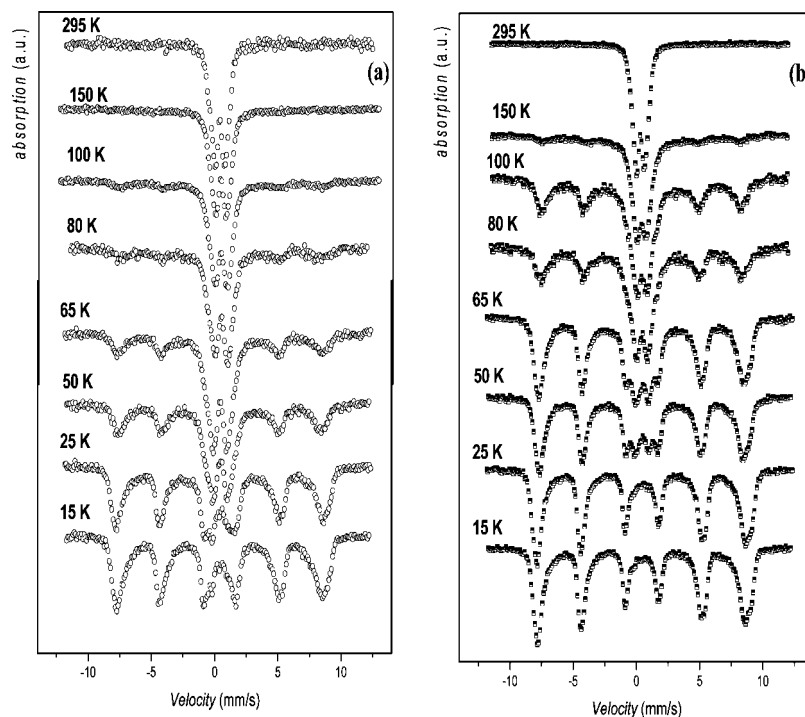
Figure 7. Mössbauer spectra in zero magnetic field, recorded in the temperature range 5–295 K for samples N5 (a, ○) and N10 (b, ■).
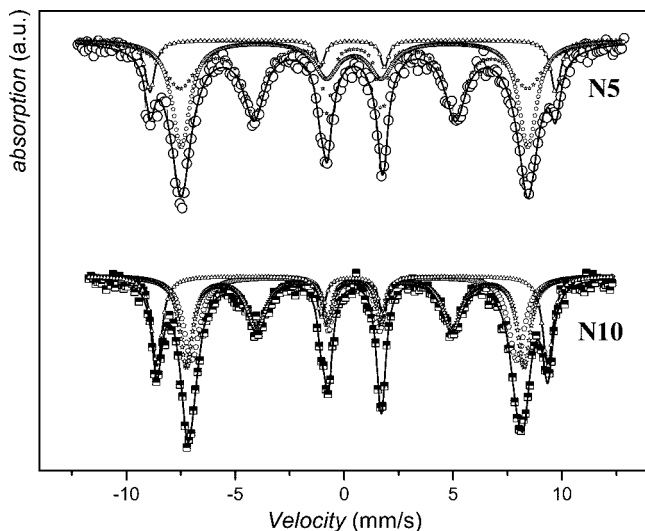
Figure 8. Mössbauer spectra recorded at 6 K in an external magnetic field of 6 T, applied parallel to the γ-ray direction for samples N5 (○) and N10 (■). Three sextets can be identified: sextet 1, △; sextet B, ⬠; sextet 3, ☆.

and 5 in the spectra indicates the presence of a noncollinear magnetic structure, with some spins that are not aligned parallel or antiparallel to the external magnetic field. The procedures used to fit such spectra were described in detail in our previous work.[7] Several fit procedures were used to investigate the validity of different possible models. The best result was obtained by fitting the spectra with three sextets and assuming perfect ferrimagnetic local environments for some of the iron atoms. Thus, the relative area of lines 2 and 5 was constrained to zero for two sextets corresponding to A (sextet 1) and B sites (sextet 2). A third sextet (sextet 3) was introduced to represent the ions with canted spins, and in this component the parameter $p = A_{2,5}/A_{3,4}$ was free. Table 4 gives the Mössbauer parameters for the three samples. As in previous studies,[7,27–29] sextets 2 and 3 show values of the isomer shift typical for octahedrally coordinated Fe^{3+} in spinels, but larger than that of sextet 1, which is typical for tetrahedrally coordinated Fe^{3+}. This suggests that the canted spins are mainly located in the B sites. The values of isomer shifts and hyperfine fields for the samples N15 and N10 are equal within the experimental error, and this suggests that there is no appreciable variation in the magnetic structure of the nanoparticles. The hyperfine fields for sample N5 are slightly different. The relative areas of lines 2 and 5 and the average value of canting angle are larger for N5 than that for N10.

An important difference between the samples was observed in the cationic distribution. The ratio between A (sextet 1) and

B (sextets 2 and 3) sites (α) is 0.11, 0.28, and 0.35 for the samples N5, N10, and N15, respectively. The very small value for N5 may explain why this sample shows hyperfine fields that differ from those of N10 and N15. The obtained cation distributions are reported in Table 4. It is worth pointing out that even small changes in the cationic distribution can result in significant changes of saturation magnetization and anisotropy.[30]

The different α-values can be ascribed to the fact that the self-combustion process occurs in slightly different ways in the three samples. Indeed, the thermal analysis of the precursors shows some differences. The exothermic peak corresponding to autocombustion reaction is centered at about 200 °C for N15, and it becomes broader and shifts to 220 and 230 °C for the N10 and N5 samples, respectively.[13] This behavior indicates a different speed of the particle formation and growth and might induce differences in cation distribution and spin-canting. Previous studies[9] showed than the increase in the temperature can induce a decrease of α-value. Ultrasmall particles are very sensitive to these effects, and even small differences in the thermal history of the material can induce relevant modifications in the cation distributions.[31]

Since the canted spins occupy mainly B sites, it is expected that different cation distributions result in different canting properties. Indeed, a decrease of the α-value (i.e., increase of Fe^{3+} fraction in the B sites) together with the increase of a canted spin fraction is observed from the N15 to N5 sample.

The results of Mössbauer measurements allow gaining a better insight into the results of magnetization measurements. The cation distribution, determined by Mössbauer spectra, is expected to affect the values of $\langle K_{eff} \rangle$, which have been derived from the AC susceptibility measurements. In the N5 sample, the lower fraction of Co^{2+} ions in B sites (Table 4) should give rise to a reduction of the $\langle K_{eff} \rangle$ value[7,32] compared to the other two samples. On the contrary, $\langle K_{eff} \rangle$ is found to increase with decreasing Co occupation of the B sites (i.e., moving from the N15 to the N5 sample). This indicates that other contributions are more important in determining the effective anisotropy of particles, presumably mainly the surface contribution, since $\langle K_{eff} \rangle$ increases with decreasing particle size. This is consistent with the increase of $\mu_0 H_c$ with decreasing particle size. The surface contribution to the magnetic anisotropy can be also responsible for the nonregular trend in the T_B values if only the volume anisotropy is considered. Actually, the value of T_B for N15 is closer to those of N10 and N5 than expected according to volume anisotropy (i.e., $T_B \propto KV$). The saturation magnetization value depends on the combined cation distributions, canted spin fractions, and surface effects. A steep increase of M_s at low temperature has been observed in ferrite nanoparticles, and it has been suggested that this is due to the freezing of surface-

TABLE 4: Effective Magnetic Field (B_{eff}), Isomer Shift (δ), Ratio between the Areas of the A and B Components (α), Relative Areas of Lines 2 and 5 ($A_{2,5tot}$),[a] Canting Angle ($\langle \theta \rangle$), and Cationic Distribution[b]

sample	spectral component	B_{eff} (T)	δ (mm/s)	area ratio ($\alpha = A/B$)	$A_{2,5tot}$ (%)	$\langle \theta \rangle$ (deg)	cationic distribution
N5	sextet 1 (tetr.-A site)	57.8(2)	0.39(3)	0.11(1)	32(1)	42(1)	$(Co_{0.80}Fe_{0.20})[Co_{0.20}Fe_{1.80}]O_4$
	sextet 2 (oct.-B site)	49.4(1)	0.46(2)				
	sextet 3 (canted spin)	49.5(3)	0.46(5)				
N10	sextet 1 (tetr.-A site)	55.7(3)	0.37(4)	0.28(2)	17(1)	37(1)	$(Co_{0.56}Fe_{0.44})[Co_{0.44}Fe_{1.56}]O_4$
	sextet 2 (oct.-B site)	47.0(2)	0.48(3)				
	sextet 3 (canted spin)	48.3(5)	0.53(7)				
N15	sextet 1 (tetr.-A site)	55.8(2)	0.38(2)	0.35(3)	15(1)	38(1)	$(Co_{0.48}Fe_{0.52})[Co_{0.52}Fe_{1.48}]O_4$
	sextet 2 (oct.-B site)	46.9(2)	0.47(2)				
	sextet 3 (canted spin)	48.6(2)	0.50(3)				

[a] The area of lines 2 and 5 is normalized by the total area of the spectrum. [b] Uncertainties are given in parentheses in the last digit.

canted spins.[10,33–35] The larger saturation magnetization for N10 with respect to that of N15 should mainly be determined by the decrease of α-value, as the fractions of canted spins are similar. The different M_s values for N5 and N10 can be related to differences in cation distributions as well as different fractions of noncollinear spins and differences of canting angles.

4. Conclusions

The magnetic properties of two samples consisting of CoFe$_2$O$_4$ nanoparticles of same size, 3 nm, dispersed in silica matrix at different concentrations, 5 and 10 wt %, have been investigated. For both samples, the observed magnetic behavior is that typical of an assembly of almost noninteracting superparamagnetic particles whose moments block below a given temperature. Despite the same particle size, the two samples exhibit some differences, indicating a correlation between cation distribution and magnetic properties: A concomitant increase of Fe^{3+} in B site and spin-canted fraction is observed. The larger anisotropy constant of the two samples compared to that of the N15 samples (7 nm) suggests that surface effects play a dominant role in the ultrasmall CoFe$_2$O$_4$ nanoparticles. This is confirmed by the observation of exchange bias in N5 and N10 samples due to the presence of a magnetically disordered surface shell exchange coupled to the magnetically ordered core.

References and Notes

(1) *Nanophase Materials, Synthesis, Properties, Applications*, Proceedings of the NATO Advanced Study Institute on Nanophase Materials, Synthesis, Properties, Applications, Corfu, Greece, June 20–July 2, 1993; Hadjipanays, G. C., Siegel, R. W., Eds.; Kluwer Academic Publishers: Boston, 1994.

(2) *Magnetic Properties of Fine Particles*, Proceedings of the International Workshop on Studies of Magnetic Properties of Fine Particles and Their Relevance to Materials Science, Rome, Italy, Nov 4–8, 1991; Dormann, J. L., Fiorani, D., Eds.; North-Holland: Amsterdam, 1992.

(3) Dormann, J. L.; Fiorani, D.; Tronc, E. In *Advances in Chemical Physics*; Prigogine, I., Rice, S. A., Eds.; Wiley: New York, 1997; Vol. 98, p 283.

(4) Kodama, R. H.; Berkowitz, A. E. *Phys. Rev. B* **1999**, *59*, 6321.

(5) Coey, J. M. D. *Phys. Rev. Lett.* **1971**, *27*, 1140.

(6) Morrish, A. H.; Haneda, K. *J. Magn. Magn. Mater.* **1983**, *35*, 105.

(7) Cannas, C.; Fiorani, D.; Musinu, A.; Peddis, D.; Piccaluga, G.; Rasmussen, H. K.; Mørup, S. *J. Chem. Phys.* **2006**, *125*, 164714.

(8) Morales, M. P.; Serna, C. J.; Bødker, F.; Mørup, S. *J. Phys.: Condens. Matter* **1997**, *9*, 5461.

(9) Chen, J. P.; Klabunde, K. J.; Hadjipanayis, G. C.; Devlin, E.; Kostikas, A. *Phys. Rev. B* **1996**, *54*, 9288.

(10) De Biasi, E.; Zysler, R. D.; Ramos, C. A.; Romero, H. *Physica B* **2002**, *320*, 203.

(11) Mørup, S.; Bødker, F.; Hendriksen, P. V.; Linderoth, S. *Phys. Rev. B* **1995**, *52*, 287.

(12) Fiorani, D.; Dormann, J. L.; Cherkaoui, R.; Tronc, E.; Lucari, F.; D'Orazio, F.; Spinu, L.; Noguès, M.; Garcia, A.; Testa, A. M. *J. Magn. Magn. Mater.* **1999**, *196–197*, 143.

(13) Cannas, C.; Musinu, A.; Peddis, D.; Piccaluga, G. *Chem. Mater.* **2006**, *18*, 3835.

(14) Gittleman, J. L.; Abels, B.; Bozowski, S. *Phys. Rev. B* **1974**, *9*, 3891.

(15) Néel, L. *Ann. Geophys.* **1949**, *5*, 99.

(16) Hansen, M. F.; Mørup, S. *J. Magn. Magn. Mater.* **1999**, *203*, 214.

(17) Del Bianco, L.; Fiorani, D.; Testa, A. M.; Sonetti, E.; Savini, L.; Signorini, E. *Phys. Rev. B* **2002**, *66*, 174418.

(18) Dormann, J. L.; D'Orazio, F.; Lucari, F.; Tronc, E.; Prené, P.; Jolivet, J. P.; Fiorani, D.; Cherkaoui, R.; Noguès, M. *Phys. Rev. B* **1996**, *53*, 14291.

(19) Zhang, J.; Boyd, C.; Luo, W. *Phys. Rev. Lett.* **1996**, *77*, 390.

(20) Chantrell, R. W.; El-Hilo, M.; O'Grady, K. *IEEE Trans. Magn.* **1991**, *27*, 3570.

(21) Rondinone, A. J.; Liu, C.; Zhang, Z. J. *J. Phys. Chem. B* **2001**, *105*, 7967.

(22) Rondinone, A. J.; Samia, A. C. S.; Zhang, Z. J. *Appl. Phys. Lett.* **2000**, *76*, 3624.

(23) Morrish, A. H. *The Physical Principles of Magnetism*; Wiley: New York, 1965; p 394.

(24) Del Bianco, L.; Hernando, A.; Multigner, M.; Prados, C.; Sánchez-López, J. C.; Fernández, A.; Conde, C. F.; Conde, A. *J. Appl. Phys.* **1988**, *84*, 2189.

(25) Vandenberghe, R. E.; De Grave, E. In *Mössbauer Spectroscopy Applied to Inorganic Chemistry*; Grandjean, F.; Long, G. J., Eds.; Plenum Press: New York, 1984; Vol. 3, p 59.

(26) Helgason, Ö.; Greneche, J. M.; Berry, F. J.; Mørup, S.; Mosselmans, F. *J. Phys.: Condens. Matter* **2001**, *13*, 10785.

(27) Helgason, Ö.; Rasmussen, H. K.; Mørup, S. *J. Magn. Magn. Mater.* **2006**, *302*, 413.

(28) Anhøj, T. A.; Bilenberg, B.; Thomsen, B.; Damsgaard, C. D.; Rasmussen, H. K.; Jacobsen, C. S.; Mygind, J.; Mørup, S. *J. Magn. Magn. Mater.* **2003**, *260*, 115.

(29) Haneda, K.; Morrish, A. H. *J. Appl. Phys.* **1988**, *8*, 4258.

(30) West, A. R. *Solid State Chemistry and Its Applications*; Wiley: New York, 1984.

(31) Tung, L. D.; Kolesnichenko, V.; Caruntu, D.; Chou, N. H.; O'Connor, C. J.; Spinu, L. *J. Appl. Phys.* **2003**, *93*, 7486.

(32) Hu, G.; Choi, J. H.; Eom, C. B.; Harris, V. G.; Suzuki, Y. *Phys. Rev. B* **2000**, *62*, 779.

(33) Aquino, R.; Depeyrot, J.; Sousa, M. H.; Tourinho, F. A.; Dubois, E.; Perzynski, R. *Phys. Rev. B* **2005**, *72*, 184435.

(34) Alves, C. R.; Aquino, R.; Depeyrot, J.; Cotta, T. A. P.; Sousa, M. H.; Tourinho, F. A.; Rechenberg, H. R.; Goya, G. F. *J. Appl. Phys.* **2006**, *99*, 08M905.

(35) Tronc, E.; Ezzir, A.; Cherkaoui, R.; Chanéac, C.; Noguès, M.; Kachkachi, H.; Fiorani, D.; Testa, A. M.; Grenèche, J. M.; Jolivet, J. P. *J. Magn. Magn. Mater.* **2000**, *221*, 63.